

# Probing nuclear expansion dynamics with $\pi^-/\pi^+$ -spectra <sup>\*†</sup>

S. Teis, W. Cassing, M. Effenberger, A. Hombach, U. Mosel and Gy. Wolf <sup>‡</sup>

Institut für Theoretische Physik, Universität Giessen

D-35392 Giessen, Germany

September 26, 2018

## Abstract

We study the dynamics of charged pions in the nuclear medium via the ratio of differential  $\pi^-$ - and  $\pi^+$ -spectra in a coupled-channel BUU (CBUU) approach. The relative energy shift of the charged pions is found to correlate with the pion freeze-out time in nucleus-nucleus collisions as well as with the impact parameter of the heavy-ion reaction. Furthermore, the long-range Coulomb force provides a 'clock' for the expansion of the hot nuclear system. Detailed comparisons with experimental data for  $Au + Au$  at 1 GeV/A and  $Ni + Ni$  at 2.0 GeV/A are presented.

PACS: 25.75. +r

Keywords: Relativistic Heavy-Ion Collisions

---

\*Supported by BMBF and GSI Darmstadt

†part of the PhD thesis of S. Teis

‡Supported by Hungarian OTKA Funds T16594,T16249

# 1 Introduction

The meson-baryon dynamics in relativistic nucleus-nucleus collisions is of particular interest since one expects to learn about the hadron properties and abundancies in hot and dense nuclear matter. Whereas dileptons from  $\rho^0$  decays or  $\pi^+\pi^-$  annihilation provide information on the timescale of 1.3 fm/c in the high density phase [1, 2, 3, 5, 6, 7], pion correlations can be used to learn about the freeze-out volume of the pions during the expansion phase. Whereas the latter method has been extensively explored in nucleus-nucleus collisions at AGS and SPS energies [4], pion correlation measurements are less promising at SIS energies due to the much lower pion multiplicities achieved at 1 - 2 GeV/A. Alternatively, one might here use the kinematic shift of  $\pi^-$  to  $\pi^+$  spectra due to the long range Coulomb force [8] in order to learn about the baryon expansion dynamics at the production time of those pions that no longer interact with the baryons and are identified experimentally [9, 10].

In this paper we investigate more systematically the pion dynamics in the time dependent Coulomb field generated by all charged hadrons in nucleus-nucleus collisions from 1 - 2 GeV/A for systems at SIS. Our analysis is carried out within the coupled-channel BUU (CBBU) transport approach [11] which is briefly described in Section 2. In Section 3 we analyse the correlation between Coulomb effects and the pion production time as a function of the pion momentum in the cms and study the sensitivity of the  $\pi^-/\pi^+$  spectra to the reaction geometry of the heavy-ion collision. Detailed comparisons with experimental data for the  $\pi^-/\pi^+$  ratio are, furthermore, presented for  $Au + Au$  at 1 GeV/A and  $Ni + Ni$  at 2.0 GeV/A. Section 4, finally, concludes our study with a summary and a discussion of open problems.

## 2 The CBUU-Model

### 2.1 Basic equations

For our present study we use the CBUU-transport-model [11] to describe the time evolution of relativistic heavy-ion collisions. In this approach, apart from the nucleon and the  $\Delta(1232)$ , all nucleon resonances up to masses of  $1.95 \text{ GeV}/c^2$  are taken into account as well as the mesons  $\pi$ ,  $\eta$ ,  $\rho$  and  $\sigma$ . While the  $\pi$ -,  $\eta$ - and  $\rho$ -mesons correspond to physical particles, the  $\sigma$ -meson is introduced to describe correlated pion-pairs with total spin  $J = 0$ . For the baryons as well as for the mesons all isospin degrees of freedom are treated explicitly. The hadrons included in our model obey a set of coupled transport equations for their one-body phase-space distributions  $f_i(\vec{r}, \vec{p}, t)$  [12, 13, 14, 16]:

$$\begin{aligned} & \frac{\partial f_1(\vec{r}, \vec{p}_1, t)}{\partial t} + \left\{ \frac{\vec{p}_1}{E_1} + \frac{m_1^*(\vec{r}, \vec{p}_1)}{E_1} \vec{\nabla}_p U_1(\vec{r}, \vec{p}_1) \right\} \vec{\nabla}_r f_1(\vec{r}, \vec{p}_1, t) \\ & \quad + \left\{ -\frac{m_1^*(\vec{r}, \vec{p}_1)}{E_1} \vec{\nabla}_r U(\vec{r}, \vec{p}_1) - q_1 \vec{\nabla}_r V_C(\vec{r}) \right\} \vec{\nabla}_p f_1(\vec{r}, \vec{p}_1, t) \\ & = \sum_{2,3,4} \frac{g}{(2\pi)^3} \int d^3 p_2 \int d^3 p_3 \int d\Omega_4 \delta^3(\vec{p}_1 + \vec{p}_2 - \vec{p}_3 - \vec{p}_4) \end{aligned}$$

$$\begin{aligned}
& \times (v_{34} \frac{d\sigma_{34 \rightarrow 12}}{d\Omega} f_3(\vec{r}, \vec{p}_3, t) f_4(\vec{r}, \vec{p}_4, t) \bar{f}_1(\vec{r}, \vec{p}_1, t) \bar{f}_2(\vec{r}, \vec{p}_2, t)) \\
& - v_{12} \frac{d\sigma_{12 \rightarrow 34}}{d\Omega} f_1(\vec{r}, \vec{p}_1, t) f_2(\vec{r}, \vec{p}_2, t) \bar{f}_3(\vec{r}, \vec{p}_3, t) \bar{f}_4(\vec{r}, \vec{p}_4, t)). \quad (1)
\end{aligned}$$

The l.h.s. of eq. (1) represents the relativistic Vlasov-equation for hadrons with charge  $q_i$  moving in a scalar momentum-dependent field  $U_i(\vec{r}, \vec{p}_i)$  [11] as well as in the electromagnetic potential  $V_C(\vec{r})$ , where  $\vec{r}$  and  $\vec{p}_i$  stand for the spatial and momentum coordinates of the hadrons, respectively. The effective mass  $m_i^*(\vec{r}, \vec{p}_i)$  in eq. (1) includes the restmass  $m_i^0$  of hadron  $i$  as well as a scalar mean-field potential  $U_i(\vec{r}, \vec{p}_i)$ , i.e.

$$m_i^*(\vec{r}, \vec{p}_i) = m_i^0 + U_i(\vec{r}, \vec{p}_i). \quad (2)$$

Since in our model the mesons will be propagated as free particles with respect to the nuclear interaction, their effective masses are equal to their restmasses, i.e.  $U_i(\vec{r}, \vec{p}_i) \equiv 0$  for mesons. The r.h.s. (i.e. the collision integral) of eq. (1) describes the changes of  $f_i(\vec{r}, \vec{p}_i, t)$  due to two-body collisions among the hadrons ( $h_1 + h_2 \leftrightarrow h_3 + h_4$ ) and two-body decays of baryonic and mesonic resonances. Furthermore,  $v_{12} \frac{d\sigma_{12 \rightarrow 34}}{d\Omega}$  is the in-medium collision rate,  $\bar{f}_i = 1 - f_i$  ( $i = 1, \dots, 4$ ) are the Pauli-blocking factors for fermions and  $v_{12}$  is the relative velocity between the colliding hadrons  $h_1$  and  $h_2$  in their center-of-mass system. In the collision integrals describing two-body decays of resonances one has to replace the product (relative velocity  $\times$  cross-section  $\times f_2$ ) by the corresponding decay rate and to introduce the proper fermion blocking factors in the final channel. The factor  $g$  in (1) stands for the spin degeneracy of the particles participating in the collision whereas  $\sum_{2,3,4}$  stands for the sum over the isospin degrees of freedom of particles 2, 3 and 4. We include the following elastic and inelastic baryon-baryon collisions, inelastic meson-baryon collisions as well as meson-meson collisions (for a detailed discussion of the cross sections employed cf. [11]):

$$\begin{aligned}
NN & \longleftrightarrow NN \\
NR & \longleftrightarrow NR \\
NN & \longleftrightarrow NR \\
NR & \longleftrightarrow NR' \\
NN & \longleftrightarrow \Delta(1232)\Delta(1232) \\
R & \longleftrightarrow N\pi \\
R & \longleftrightarrow N\pi\pi \\
R & \longleftrightarrow \Delta(1232)\pi, N(1440)\pi, N\rho, N\sigma \\
N(1535) & \longleftrightarrow N\eta \\
NN & \longleftrightarrow NN\pi \\
\rho & \longleftrightarrow \pi\pi \quad (\text{p-wave}) \\
\sigma & \longleftrightarrow \pi\pi \quad (\text{s-wave}), \quad (3)
\end{aligned}$$

where  $R$  and  $R'$  represent all baryonic resonances up to a mass of 1.95 GeV/c<sup>2</sup> [11].

## 2.2 The Coulomb Potential

Charged baryons and mesons are propagated in the electromagnetic field generated by the 4-current of all charged particles. Since our numerical studies did not indicate any sensitivity to the hadron trajectories from the time dependent magnetic fields, we only discuss the effects of the time-like component (i.e.  $V_C$ ) in the following. The Coulomb potential in our transport model is evaluated by solving the static Poisson-equation in three dimensions

$$-\left(\frac{\partial^2}{\partial x^2} + \frac{\partial^2}{\partial y^2} + \frac{\partial^2}{\partial z^2}\right)V_C(x, y, z) = 4\pi\alpha\hbar c \rho_C(x, y, z) \quad (4)$$

( $\alpha = 1/137$ ) in every time-step of the calculation where all charged particles present contribute to the charge density  $\rho_C(x, y, z)$ . The Poisson-equation (4) is integrated by means of the *Alternating-Direction Implicit Iterative* (ADI-)algorithm [17, 18], where the boundary conditions are obtained by a multipole expansion up to the quadrupole moment of the Coulomb potential. Since the mesons are propagated as free particles with respect to the nuclear mean-field, the Coulomb force

$$\vec{F}_c(\vec{r}) = -q\vec{\nabla}_r V_C(\vec{r}) \quad (5)$$

(besides the Lorentz force from the magnetic field) is the only force acting on a meson with charge  $q$ . As noted before, the curl of the spatial components of the vector potential is found to be small in the overlap regime of the colliding ions and can be neglected within the numerical accuracy achieved. For charged baryons  $F_c$  represents a force in addition to the nuclear force from the scalar mean-field potential  $U(\vec{r}, \vec{p})$ ,

$$\begin{aligned} \frac{d\vec{r}_i(t)}{dt} &= \frac{\vec{p}_i}{E_i} + \frac{m_i^*}{E_i} \vec{\nabla}_p U(\vec{r}_i, \vec{p}_i(t)) \\ \frac{d\vec{p}_i(t)}{dt} &= -\frac{m_i^*}{E_i} \vec{\nabla}_r U(\vec{r}_i, \vec{p}_i(t)) - q_i \vec{\nabla} V_C(\vec{r}_i), \end{aligned} \quad (6)$$

however, is of minor importance here.

## 3 Coulomb analysis of pion spectra

In the following we investigate the Coulomb-effects on charged pion spectra in heavy-ion collisions in the SIS energy range. We especially look at the correlation between the Coulomb-forces acting on charged pions and their freeze-out times and freeze-out densities, respectively. Finally, we present pion spectra and  $\pi^-/\pi^+$  ratios from our transport calculation for  $Au + Au$  at 1 GeV/A and  $Ni + Ni$  at 2.0 GeV/A which are studied experimentally at SIS.

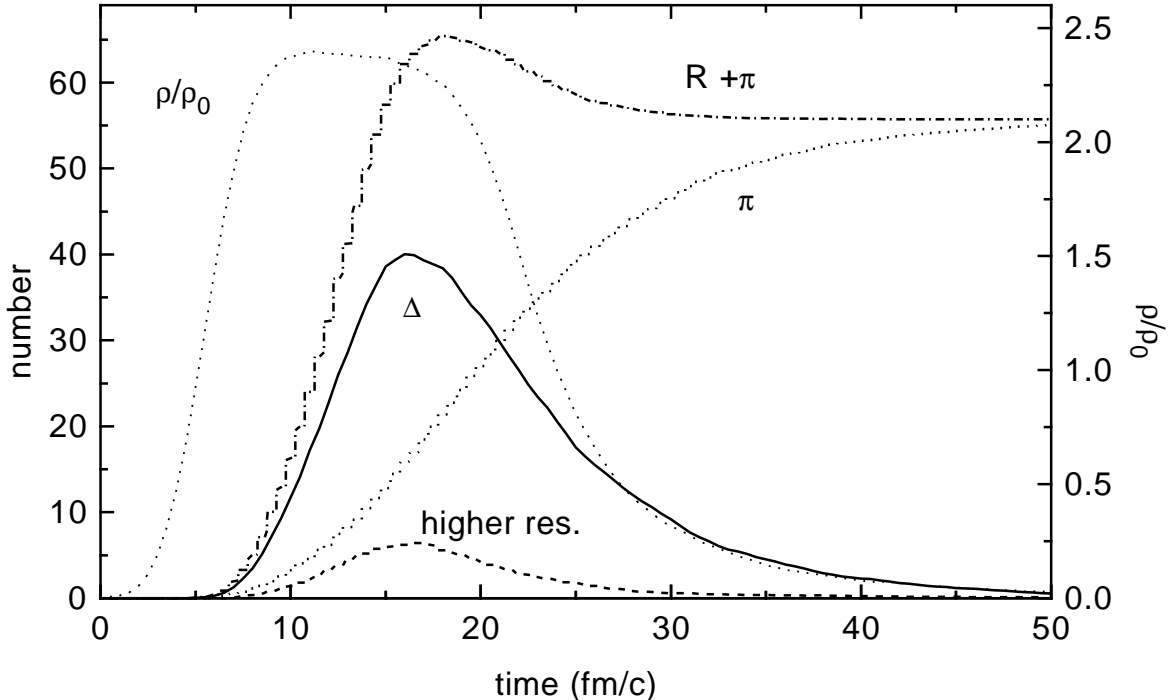


Figure 1: Number of particles in the transport calculation as a function of time for the reaction  $Au + Au$  at 1.0 GeV/A and impact parameter  $b = 0$  fm: solid line:  $\Delta(1232)$ ; dashed line: sum of all higher resonances; dotted line: pions; dash-dotted line: sum of baryonic resonances and pions. The short-dashed line shows the baryon density in a volume of  $1 fm^3$  in the center of the CMS of the colliding heavy-ions.

### 3.1 Correlation between Coulomb-effects and pion production times

In the high density phase of a heavy-ion collision in the SIS-energy range baryonic resonances like the  $\Delta(1232)$ ,  $N(1440)$ ,  $N(1535)$  etc. are excited in nucleon-nucleon collisions or via multi-step processes in pion-nucleon or resonance-nucleon collisions. These excited baryonic resonances then can be deexcited in collisions with nucleons (e.g.  $\Delta(1232)N \rightarrow NN$ ) or decay into nucleons and pions. If these decays take place in the high density phase of the heavy-ion reaction the emerging pions are likely to be absorbed again, but if the decays occur in the expansion phase of the reaction or in low density regimes, i.e. at the surface of the reaction volume, the pions may escape from the nuclear medium (freeze-out).

This line of argument is supported by fig. 1 where we show the number of baryonic resonances and pions present in our transport calculation as a function of time for a central ( $b = 0$  fm)  $Au + Au$  collision at 1.0 GeV/A. The short-dashed line indicates

the baryon density in a volume of  $1 \text{ fm}^3$  in the center of the CMS of the two colliding nuclei. The population of the baryonic resonances sets in as the density in the overlap zone of the colliding heavy-ions increases and reaches its maximum at the end of the high density phase at about  $15 - 20 \text{ fm}/c$ . This holds for the  $\Delta(1232)$  (solid line) as well as for the higher resonances (dashed and dotted lines). For the pions, however, we obtain a different picture. The number of pions increases monotonically with time and reaches its maximum (asymptotic) value at the end of the reaction, which is about a factor 1.2 higher than the maximum number of  $\Delta$ 's in the high density phase. This implies that most of the pions observed at the end of the heavy-ion reaction stem from resonances decaying in the expansion phase of the reaction.

In order to discuss this effect more quantitatively we show in fig. 2 the number of asymptotically observed pions as a function of their freeze-out times for CMS momenta of 0.2 (solid line), 0.6 (dashed line) and 1.0 GeV/c (dotted line) for a  $Au + Au$  collision at 1.0 GeV/A in central collisions ( $b = 0 \text{ fm}$ ). The production of pions in all three kinematical regions yields about 10% of its maximum at  $t \approx 15 \text{ fm}/c$ , reaches its maximum between 20 and 30  $\text{fm}/c$  and then decreases with time. Since the production of pions with low momenta requires less energy than the creation of high momentum pions, there are quantitative differences in the production times of pions in the different kinematical regimes<sup>1</sup>. Pions with low momenta are already produced in the beginning of the overlap of both nuclei while the production of pions with high momenta starts only if there is enough energy density piled-up in order to produce them. For a similar reason the relative production rate of high momentum pions falls off more quickly with time than that of pions with low momenta. In general, the hard pions stem dominantly from the heavier baryonic resonances [11]. Light resonances live on average longer than heavy resonances since their decay width is smaller than that of heavy resonances. This is particularly true for the  $\Delta$  whose momentum-dependent width leads to a rather long lifetime for low mass  $\Delta$ -resonances. A second reason is that light resonances can be populated not only in the compressed phase of a heavy-ion reaction but also in less energetic nucleon-nucleon collisions in the expansion phase of the reaction while the creation of heavy resonances - equivalent to the production of hard pions - needs more energetic two-body collisions which are only present in the high density phase of the heavy-ion collision. Due to this fact we observe that the maxima of the pion-distributions in fig. 2 are shifted to smaller times  $t$  as the pions become harder.

This can be seen more quantitatively in fig. 3 where the average production time of pions produced in central events is shown as a function of their momentum in the CMS of the two colliding heavy-ions for the reaction  $Au + Au$  at 1.0 GeV/A. The squares indicate the result of the CBUU-calculation and the solid line corresponds to a linear fit to the calculated results. From this figure we can infer that soft pions are emitted on average approximately 10  $\text{fm}/c$  later than hard pions with momenta of about 1.0 GeV/c. During this time the baryonic matter expands before the emission of the soft pions. Thus the production density for hard pions is on average

---

<sup>1</sup>The 'production' time here is defined as the time when the  $\Delta$  decays into a nucleon and a free pion that propagates out to the detector without any further strong interactions.

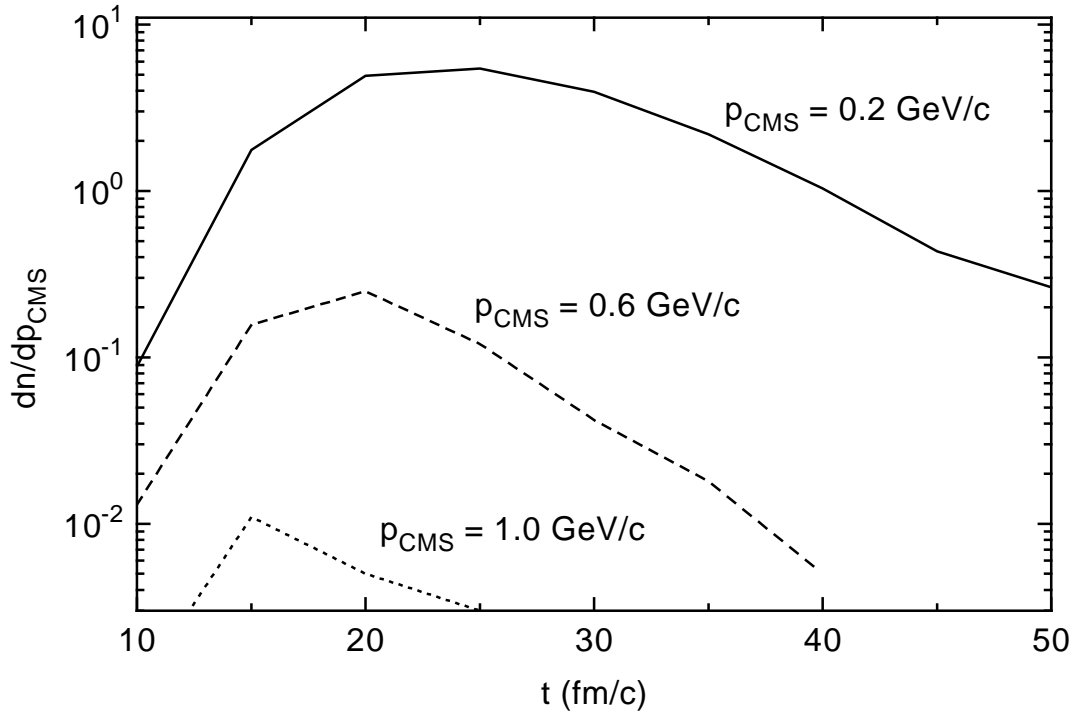


Figure 2: Number of emerging pions as a function of their final production time for  $Au + Au$  at 1.0 GeV/A taking into account only central events ( $b = 0$  fm) for different CMS pion momenta; solid line:  $p_{cms} = 0.2$  GeV/c, dashed line:  $p_{cms} = 0.6$  GeV/c, dotted line:  $p_{cms} = 1.0$  GeV/c.

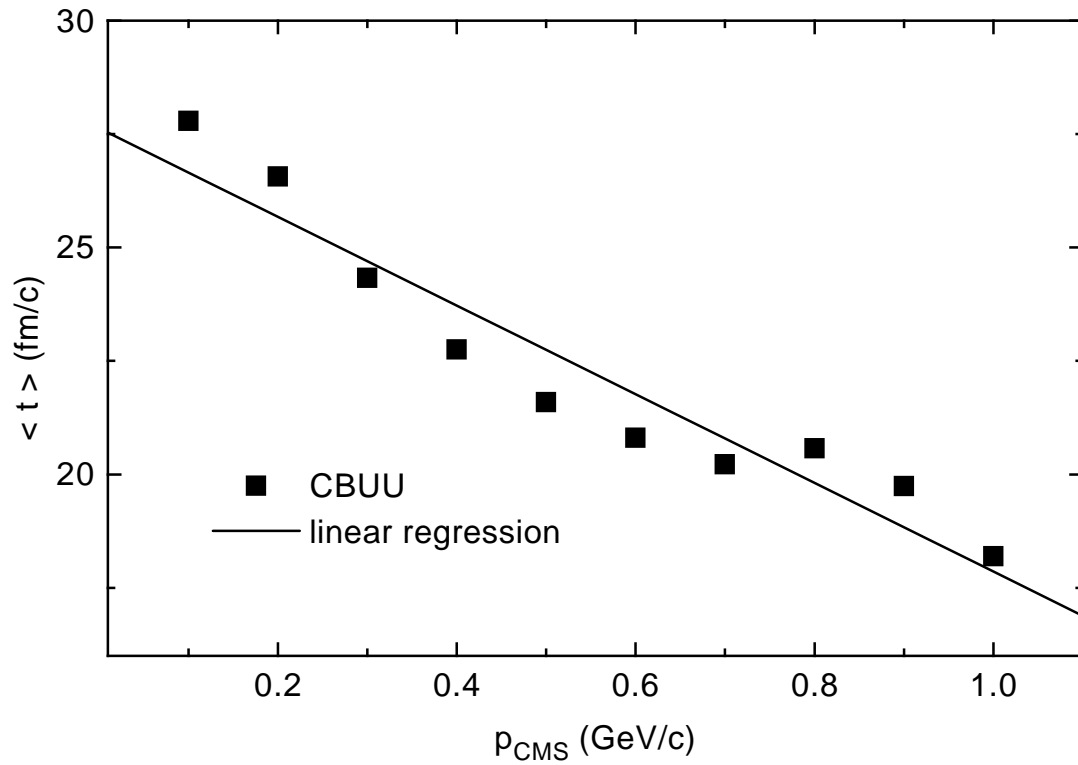


Figure 3: Average production time of pions as a function of their CMS momentum for  $Au + Au$  at 1.0 GeV/A taking into account only central events ( $b = 0$  fm); squares: results of the CBUU-calculation, solid line: linear fit to the CBUU-results.



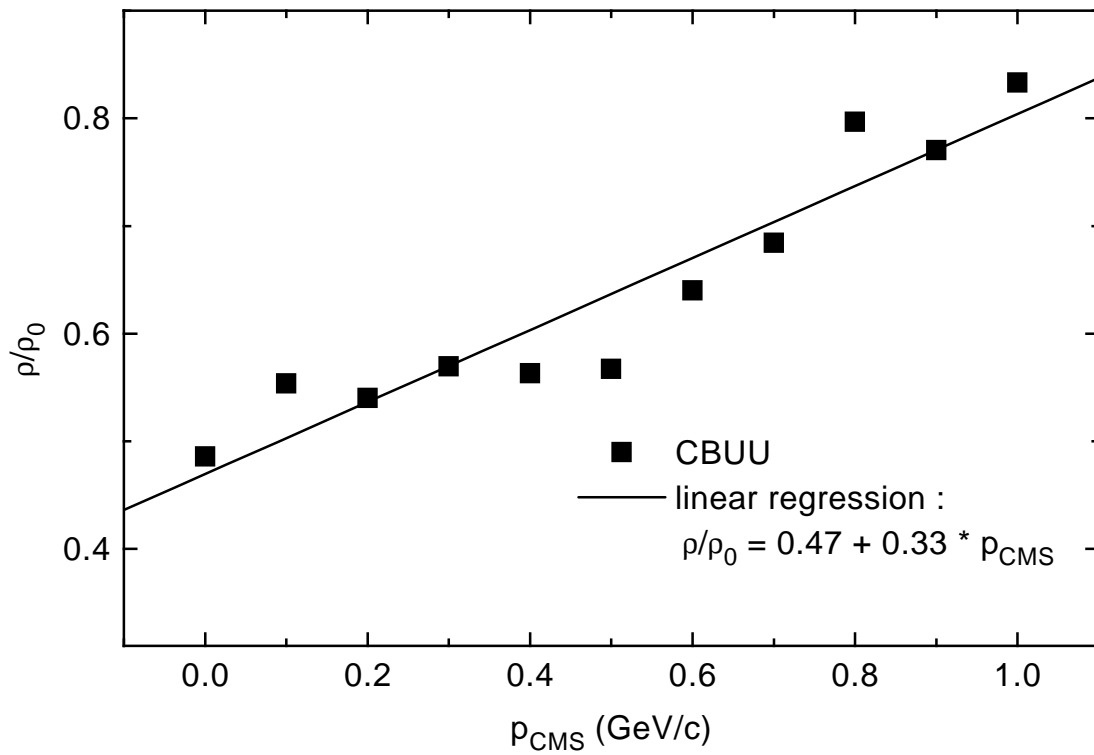


Figure 4: Average production density of pions as a function of their CMS momentum for  $Au + Au$  at 1.0 GeV/A taking into account all events ( $0 \leq b \leq 16$  fm); squares: results of the CBUU-calculation, solid line: linear fit to the CBUU-results.

higher than that of soft pions.

The relation between the average production density and the pion momentum in the CMS of the heavy-ion reaction is depicted in fig. 4 for the reaction  $Au + Au$  at 1.0 GeV/A taking into account all events ( $0 \leq b \leq 16$  fm). Quantitatively we can conclude that pions with momenta of  $\approx 1.0$  GeV/c are emitted on average at  $0.8\rho_0$ . After production of the hard pions the fireball expands to  $\approx 0.5\rho_0$  before most of the soft pions are emitted. Note, that both densities are below normal nuclear matter density such that pions carry information essentially only on the low density phase of the reaction. From the linear dependence of the freeze-out density on the pion momentum we can infer that the Coulomb potential acting on the pions, when leaving the reaction zone, must also be a linear function of the pion momenta because the charge density is proportional to the baryon density. Indeed this behaviour can be found by means of our transport calculation. In the top part of fig. 5 the absolute magnitude of the average Coulomb potential felt by the pion at its production point is plotted versus the pion momentum in the CMS. The open circles indicate the potential of the  $\pi^-$  and the open triangles that for  $\pi^+$  while the solid squares denote the Coulomb potential averaged over  $\pi^+$  and  $\pi^-$ . The solid line corresponds to a linear fit to the averaged values (squares) in the momentum range between 0.1 and 1.0 GeV/c. We find that the average Coulomb potential at freeze-out increases linearly with the pion momentum except for pions with momenta below 50 MeV/c.

In the bottom part of fig. 5 we investigate how the Coulomb effects on the pion distributions change as a function of the centrality of the heavy-ion reaction: the squares and the circles show the average Coulomb potential of the pions at freeze-out as a function of their CMS momentum for peripheral and central collisions, respectively. The solid and dashed lines represent the corresponding linear fits to the values obtained from the CBUU-calculation. Fig. 5 clearly indicates that the Coulomb effects on the final pion distributions are also sensitive to the reaction geometry, i.e. pions created in peripheral collisions feel a  $\approx 15\%$  stronger Coulomb potential than those produced in central collisions. While in central collisions almost all nucleons participate in the reaction, get compressed and collectively expand again, more and more nucleons do not participate in the heavy-ion reaction as the collision becomes more peripheral with increasing impact parameter. As a consequence the pion freeze-out configuration is more compact in peripheral reactions than in central collisions such that the pions see a stronger Coulomb field when decoupling from the baryons.

By establishing a correlation between the momenta of pions emitted in heavy-ion collisions and their average production times and densities we have proven that pions are a sensitive probe to the expansion phase of heavy-ion reactions. Obviously, by measuring the pion distributions in heavy-ion collisions one cannot directly deduce their freeze-out density or their freeze-out time, but one can take advantage of the sensitivity of the pion distributions to the Coulomb potential due to the presence of charged baryons and mesons in the reaction zone by investigating the differences in the observed  $\pi^+$ - and  $\pi^-$ -spectra. This can be achieved by looking at the ratio of

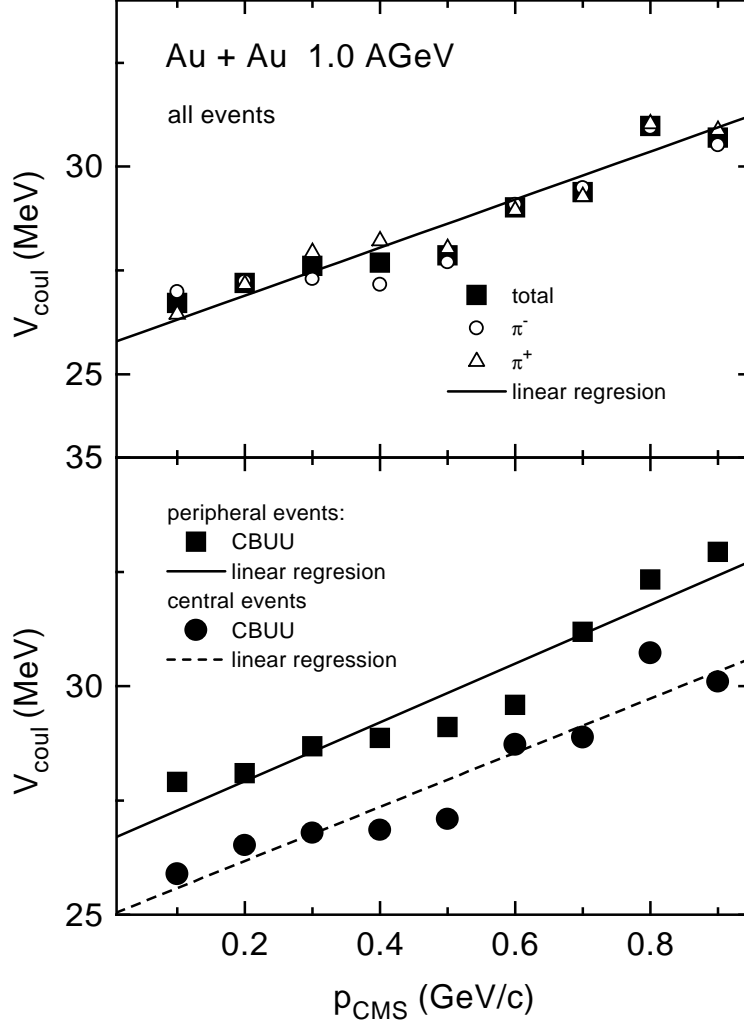


Figure 5: Average Coulomb potential of pions (at their production time) as a function of their CMS momentum for  $Au + Au$  at 1.0 GeV/A. Top: The circles represent the results obtained for  $\pi^-$  and the triangles those for  $\pi^+$ . The filled squares indicate the Coulomb potential averaged over  $\pi^+$  and  $\pi^-$  while the solid line is a linear fit to these values for pion momenta between 0.1 and 1.0 GeV/c. Here all events are taken into account ( $0 \leq b \leq 16$  fm). Bottom: The squares indicate the result for the Coulomb potential averaged over  $\pi^+$  and  $\pi^-$  for peripheral collisions ( $b > 6$  fm) and the circles represent the same for central collisions ( $0 \leq b \leq 6$  fm). The solid and the dashed line represent the corresponding linear fits to the CBUU-calculations.

the cross sections for  $\pi^+$ - and  $\pi^-$ -production. This ratio

$$R = \frac{\sigma(\pi^-)}{\sigma(\pi^+)} \quad (7)$$

is shown in fig. 6 as a function of the pion kinetic energy in the CMS of the heavy-ion collision for the reaction  $Au + Au$  at 1.0 GeV/A. The top of fig. 6 shows the results obtained with no Coulomb effects included while the bottom part depicts  $R$  obtained in a calculation including Coulomb effects. Besides the (numerical) statistical fluctuations the ratio  $R$  is constant ( $\approx 1.85 \pm 0.1$ ) when neglecting the Coulomb forces since the pions propagate freely out of the nuclear medium. Hence the  $\pi^-$  and  $\pi^+$ -spectra are not shifted relative to each other and the deviation of the ratio  $R$  from 1 reflects the isospin asymmetry of the  $Au + Au$  system which according to [15] reads,

$$R = \frac{5N^2 + NZ}{5Z^2 + NZ}, \quad (8)$$

where  $N$  and  $Z$  are the number of neutrons and protons, respectively. For a  $Au + Au$  collision eq. (8) gives  $R = 1.95$ , which is in good agreement with our transport calculation without Coulomb forces. The ratio obtained when including the Coulomb forces (bottom part of fig. 6) shows an energy-dependent behaviour. For kinetic energies of  $\approx 50$  MeV it yields a value of about 3.0 whereas with increasing pion kinetic energy the  $\pi^-/\pi^+$ -ratio decreases to about 0.8 for energies of  $\approx 300$  MeV. This energy-dependent behaviour of the ratio  $R$  can be attributed to the Coulomb potential which results in opposite forces for  $\pi^+$  and  $\pi^-$  mesons and which on average has a different strength for pions in different kinematical regions (cf. fig. 5).

### 3.2 Sensitivity of the $\pi^-/\pi^+$ -ratios to the reaction geometry

In the previous section we have shown that the variation in the Coulomb potential felt by pions due to their different production densities is the origin of the energy-dependent  $\pi^-/\pi^+$ -ratio  $R$ . In this subsection we will investigate the sensitivity of  $R$  to the reaction geometry of the heavy-ion collision. In this respect we display in fig. 7 the ratio  $R$  for the reaction  $Au + Au$  at 1.0 GeV/A as a function of the pion CMS kinetic energy for different CMS-angles of the outgoing pions. The solid line shows a fit to the total ratio  $R$ , while the dashed, the dotted and the dash-dotted lines represent the resulting  $\pi^-/\pi^+$  ratio for  $\Theta_{CMS} = 0^\circ \pm 22.5^\circ$ ,  $45^\circ \pm 22.5^\circ$  and  $90^\circ \pm 22.5^\circ$ , respectively. We observe a large ratio for soft pions emitted in forward direction while the ratios for slow pions emerging at  $\Theta_{CMS} = 45^\circ$  or  $90^\circ$  are significantly smaller. This large difference in  $R$  vanishes if the pions become harder. For pions with CMS kinetic energies of  $\approx 250$  MeV the effect has almost disappeared. This angular dependence of the ratio  $R$  can be understood within the 'participant-spectator' picture. While in central collisions almost all target and projectile nucleons participate in the collision and therefore form expanding hot nuclear matter of densities below  $\rho_0$ , in peripheral collisions the spectator matter provides more compact sources for the Coulomb potential (cf. sect. 3.1).

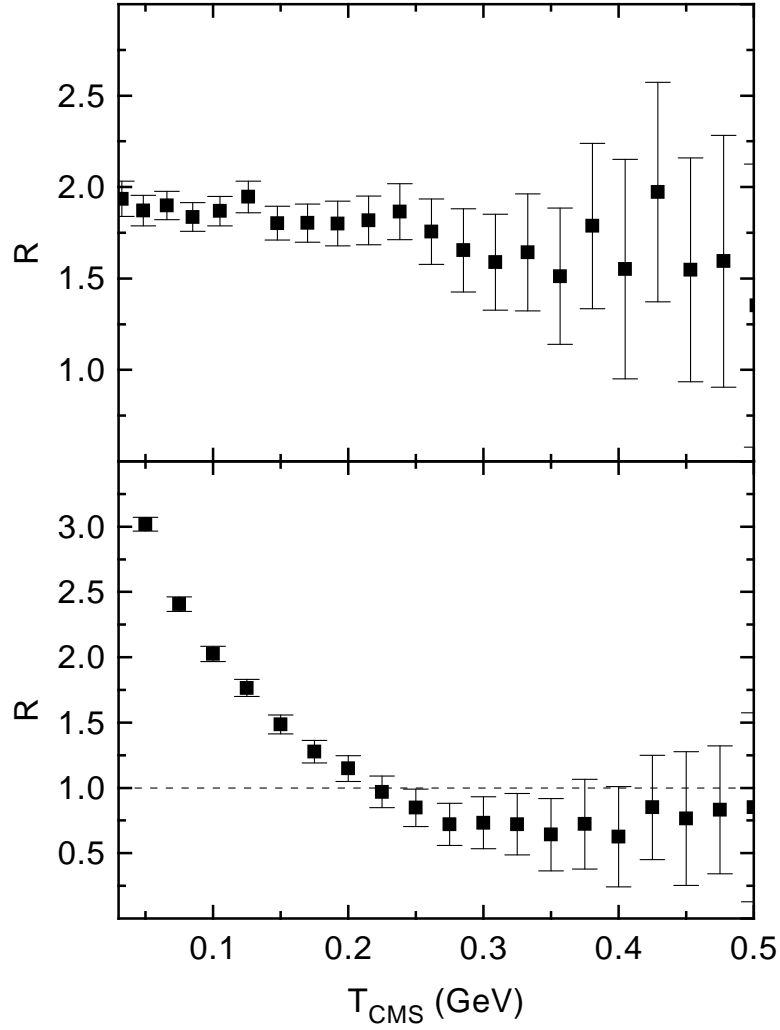


Figure 6: The ratio  $R$  as a function of the CMS pion kinetic energy for  $Au + Au$  at 1.0 GeV/A obtained in a CBUU-calculation without Coulomb effects (top) and in a calculation including the Coulomb effects (bottom). The squares denote the corresponding computational results and the errorbars account for the statistical uncertainty.

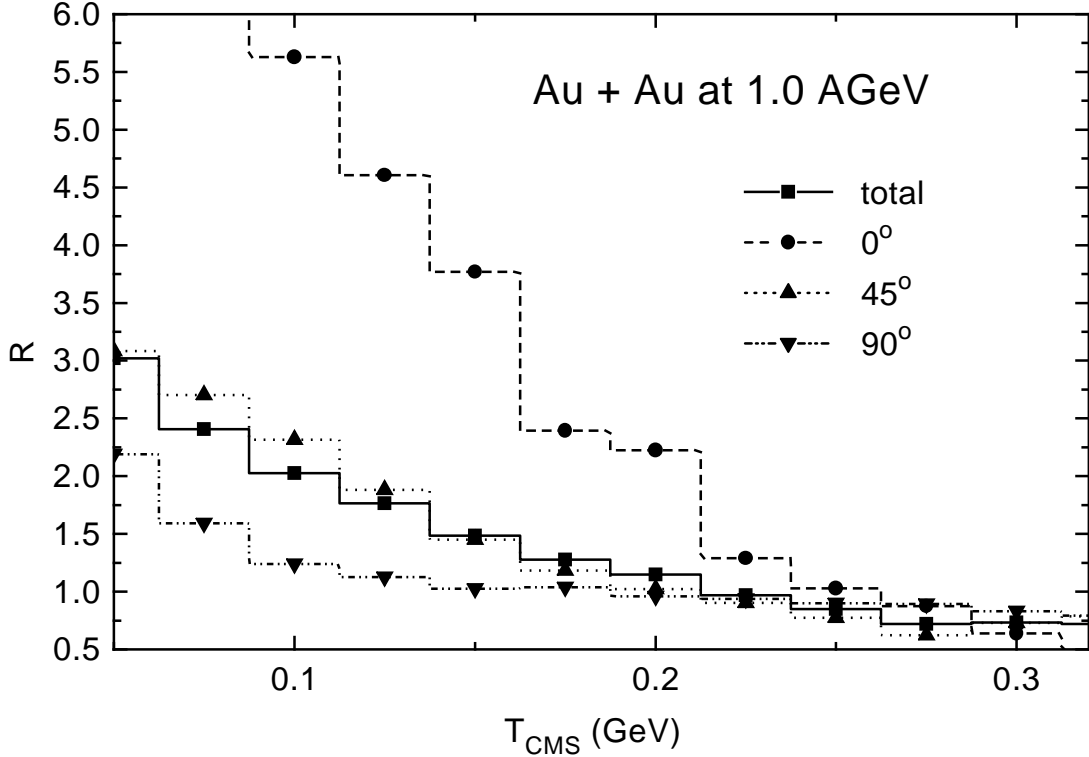


Figure 7: The ratio  $R$  for the reaction  $Au + Au$  at 1.0 GeV/A as a function of the CMS pion kinetic energy for different CMS polar angles:  $\Theta_{CMS} = 0^\circ \pm 22.5^\circ$  dashed line,  $\Theta_{CMS} = 45^\circ \pm 22.5^\circ$  dotted line,  $\Theta_{CMS} = 90^\circ \pm 22.5^\circ$  dash-dotted line. The solid line represents the ratio  $R$  integrated over all angles.

The dramatic increase in the ratio  $R$  for soft pions moving in forward direction is due to the fact that these pions move in the same direction as the spectator matter and therefore stay for a long time relatively close to the spectators. This results in a larger Coulomb distortion of the pion-spectra than for those pions leaving the reaction zone in other directions. This argument is supported by fig. 8 where in the top part we show the ratio  $R$  for pions moving in forward direction ( $\Theta_{CMS} = 0^\circ \pm 22.5^\circ$ ) for  $Au + Au$  at 1.0 GeV/A as a function of the pion kinetic CMS-energy for different event classes. The dotted histogram represents the resulting  $R$  taking into account only central ( $0 \leq b \leq 6$  fm) events, the dashed histogram corresponds to  $R$  obtained for peripheral events ( $7 \leq b \leq 16$ fm), while the solid histogram corresponds to the ratio when including all events ( $0 \leq b \leq 16$  fm). Comparing the three histograms in the top of fig. 8 we find a strong sensitivity of  $R$  to the impact parameter of the heavy-ion collision which is directly related to the impact parameter dependence of the pion Coulomb potential (cf. fig. 5). For soft pions we obtain a larger value of  $R$  for peripheral events than for central events. The size of this effect is again reduced for harder pions. This variation of

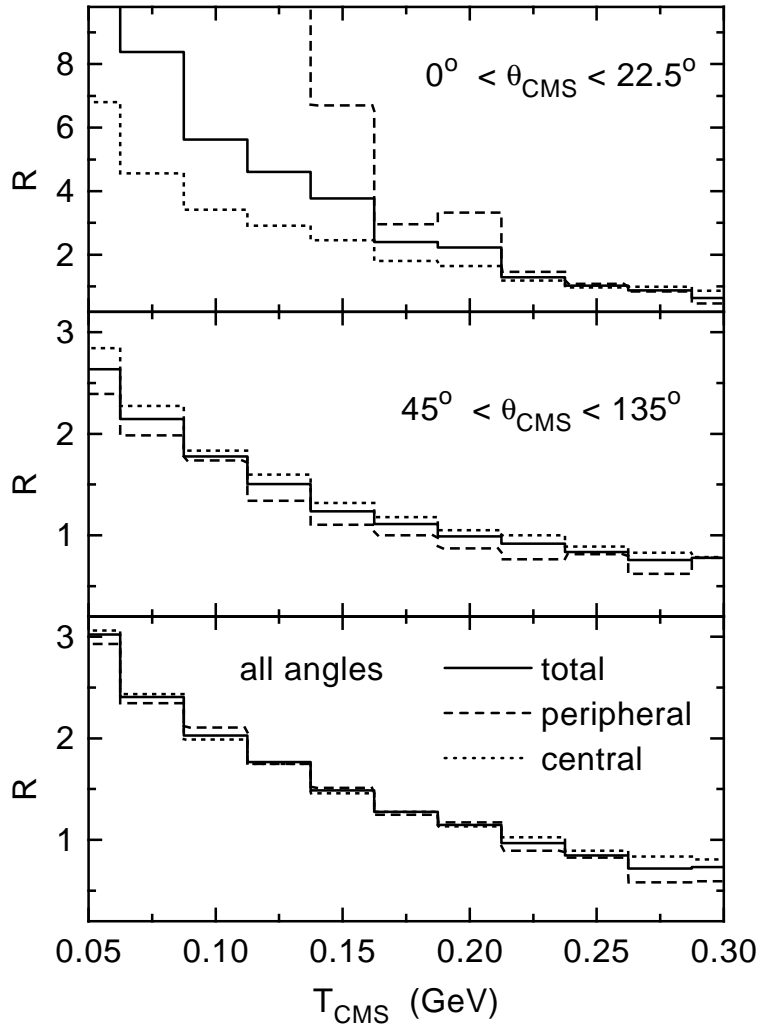


Figure 8: The ratio  $R$  for the reaction  $Au + Au$  at 1.0 GeV/A as a function of the CMS pion kinetic energy for pions with different event classes: all events: solid histogram; central events ( $0 \leq b \leq 6$  fm): dotted histogram; peripheral events ( $7 \leq b \leq 16$ fm): dashed histogram. Top: Pions moving in forward direction ( $0^\circ \leq \Theta_{CMS} \leq 22.5^\circ$ ); middle: pions leaving the reaction zone with  $45^\circ \leq \Theta_{CMS} \leq 135^\circ$ ; bottom: all pions ( $0^\circ \leq \Theta_{CMS} \leq 180^\circ$ ).

$R$  with the impact parameter of the heavy-ion collision supports the argument that the Coulomb attraction/repulsion for pions moving in forward direction is mainly due to the spectator matter. The larger amount of spectator matter in peripheral collisions leads to larger Coulomb effects than in central collisions. This dependence of the Coulomb-ratio on the impact parameter of the heavy-ion reaction is found to be reversed for pions with kinetic energies below 200 MeV when considering pions leaving the reaction zone under  $45^\circ \leq \Theta_{CMS} \leq 135^\circ$  as shown in the middle of fig. 8. The dependence of  $R$  on the impact parameter vanishes within the statistical uncertainties of our transport calculation when evaluating the Coulomb ratio  $R$  for all pions produced in the reaction (bottom part of fig. 8). This can be interpreted in the same line of argument: slow pions produced in peripheral collisions moving perpendicular to the direction of the spectators feel weaker Coulomb forces than those produced in central collisions because the spectator matter moves away from the reaction zone and thus reduces the effective Coulomb potential 'seen' by the pions.

### 3.3 Comparison with experimental data

In this subsection we compare our calculations for the inclusive pion spectra to the respective experimental data [19] and present  $\pi^-/\pi^+$  ratios for  $Au + Au$  at 1 GeV/A and Ni + Ni at 2.0 GeV/A.

First we compare our calculation with the inclusive experimental  $\pi^+$ -spectrum for Au + Au at 1.0 GeV/A for lab. angles in the range  $40^\circ \leq \Theta_{lab} \leq 48^\circ$  [19] in fig. 9. The full squares represent the experimental data of the KaoS collaboration as a function of the laboratory momentum  $p_{lab}$  whereas the histograms are the result of our calculation including the uncertainty due to the numerical statistics (shaded area). We overestimate the experimental spectrum in the range  $p_{lab} \approx 300-400$  MeV/c for the heavy system Au + Au, but reproduce the high momentum part of the spectrum reasonably well within the numerical statistics achieved. This general trend is also found in the IQMD calculations by Bass et al. [9] for this system. We note, that the high momentum tail of the spectrum basically stems for higher baryon resonances as discussed in more detail in [11].

In fig. 10 we show  $R$  for  $Au + Au$  at 1 GeV/A as a function of the pion kinetic energy in the CMS integrated over all angles (top), for  $\Theta_{lab} = 45^\circ$  (middle) and  $\Theta_{lab} = 90^\circ$  (bottom). Whereas the ratio  $R$  drops almost linearly with the pion energy up to about 0.25 GeV when integrating over all angles, its variation with the pion energy is more pronounced for the two angular cuts. Here, especially the  $\pi^-/\pi^+$  ratio at low pion energy ( $\leq 0.1$  GeV) changes significantly with laboratory angle; it drops by about 20% for  $\Theta_{lab} \approx 45^\circ$  and increases by about 20% for  $\Theta_{lab} \approx 90^\circ$  relative to the angle averaged value. Since the relative variation in the ratio  $R$  is quite pronounced, it should also clearly be seen in the respective experimental pion ratios. For comparison we also display in fig. 10 the experimental  $\pi^-/\pi^+$ -ratio from the FOPI-collaboration [21] (top: open circles) as well as the ratio obtained by the KaoS-collaboration [20] for  $40^\circ \leq \Theta_{lab} \leq 48^\circ$  (middle: open triangles). Whereas the ratio resulting from the transport calculation underestimates the FOPI-data in the



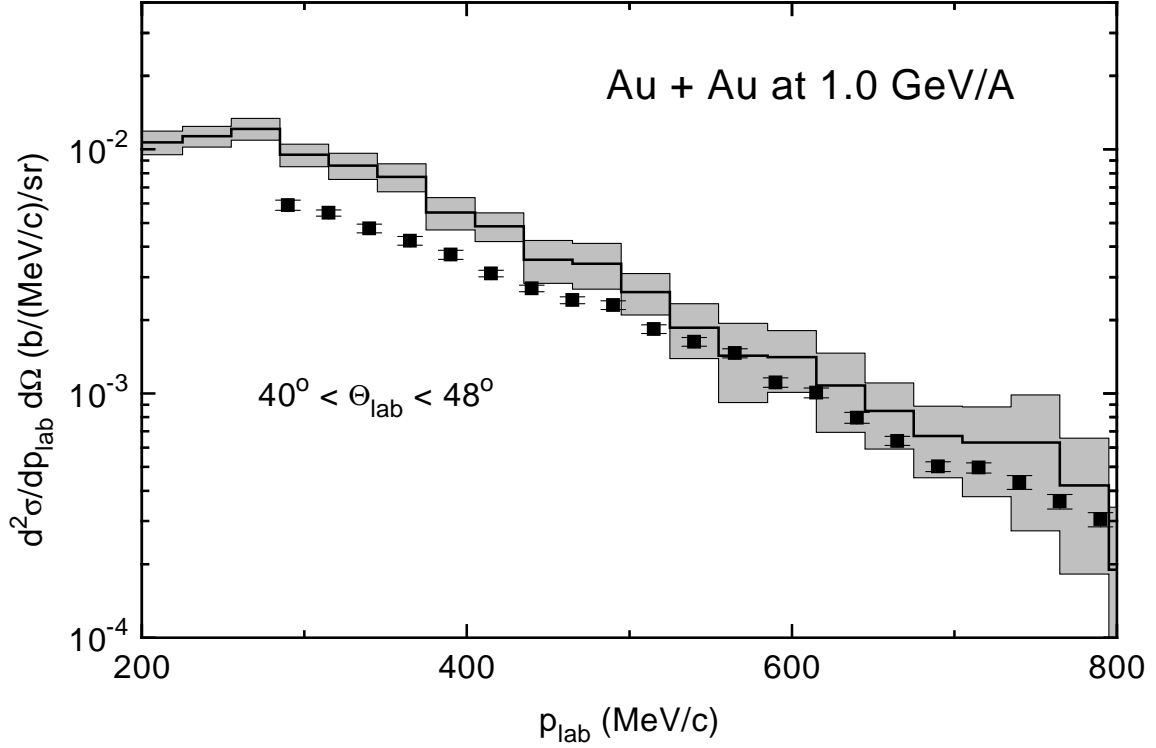


Figure 9: The inclusive  $\pi^+$ -spectrum for Au +Au at 1.0 GeV/A for lab. angles in the range  $40^\circ \leq \Theta_{lab} \leq 48^\circ$ . The full squares represent the experimental data of the KaoS collaboration [19] as a function of the laboratory momentum  $p_{lab}$  whereas the histograms are the result of our calculation including the uncertainty due to the numerical statistics (shaded area).

region of  $T_{CMS} \approx 75$  MeV it agrees within the statistical errors for higher kinetic energies. In comparison to the KaoS-data we find that the ratio is described quite well at  $T_{CMS} = 50$  MeV but is underestimated for higher pion energies.

In fig. 11 we present the  $\pi^-/\pi^+$  ratio for Ni + Ni at 2.0 GeV/A for  $85^\circ < \Theta_{CMS} < 135^\circ$ . The solid squares represent the results of our transport calculation and the open circles correspond to the  $\pi^-/\pi^+$ -ratio obtained by the FOPI-collaboration for a beam energy of 1.93 GeV/A [22]. Within the statistical errors of the calculation the data are reproduced for kinetic energies up to  $\approx 500$  MeV. Since Coulomb effects decrease with the charge of the colliding system the ratio  $R$  is close to 1 when neglecting the Coulomb forces because  $N \approx Z$ . Due to the lower charge of the system the ratio shows only a very moderate enhancement for low pion energy.

## 4 Summary

In this paper we have explored the possibility to use differential  $\pi^-/\pi^+$  ratios as a clock for the expansion dynamics of a heavy-ion reaction. The analysis is performed within the coupled-channel (CBBU) transport approach which has proven in ref. [11] to adequately describe differential pion spectra in the SIS energy regime. We have shown explicitly the correlation between the pion final production time and the baryon density or Coulomb potential that is seen by the pions at freeze-out. Furthermore, a sizeable correlation between the pion production time and the pion momentum is found due to the strong interaction dynamics.

The different Coulomb potentials seen by slow/fast pions in different directions with respect to the beam axis and for different impact parameter of the heavy-ion collisions directly induce sizeable variations in the  $\pi^-/\pi^+$  ratios especially for low pion momenta. These ratios can be measured directly by the FOPI and KaoS collaborations at GSI; detailed predictions for  $Au + Au$  at 1 GeV/A have been made in this context and are awaiting further experimental control.

So far, we have performed our analysis without including any selfenergies for the pions while assuming the mean-field potentials to be the same for all baryons. From the exploratory study in ref. [23] we know, that selfenergy effects show up dominantly at low pion momenta in the CMS. However, since such hadronic selfenergies are approximately the same for  $\pi^+$  and  $\pi^-$  mesons, their effect should cancel out when considering the ratio of the differential spectra. Precise experimental data will be very helpful in clarifying this question.

## Acknowledgements

The authors like to thank A. Wagner, C. Sturm and H. Oeschler for clarifying discussions throughout the course of this study.

## References

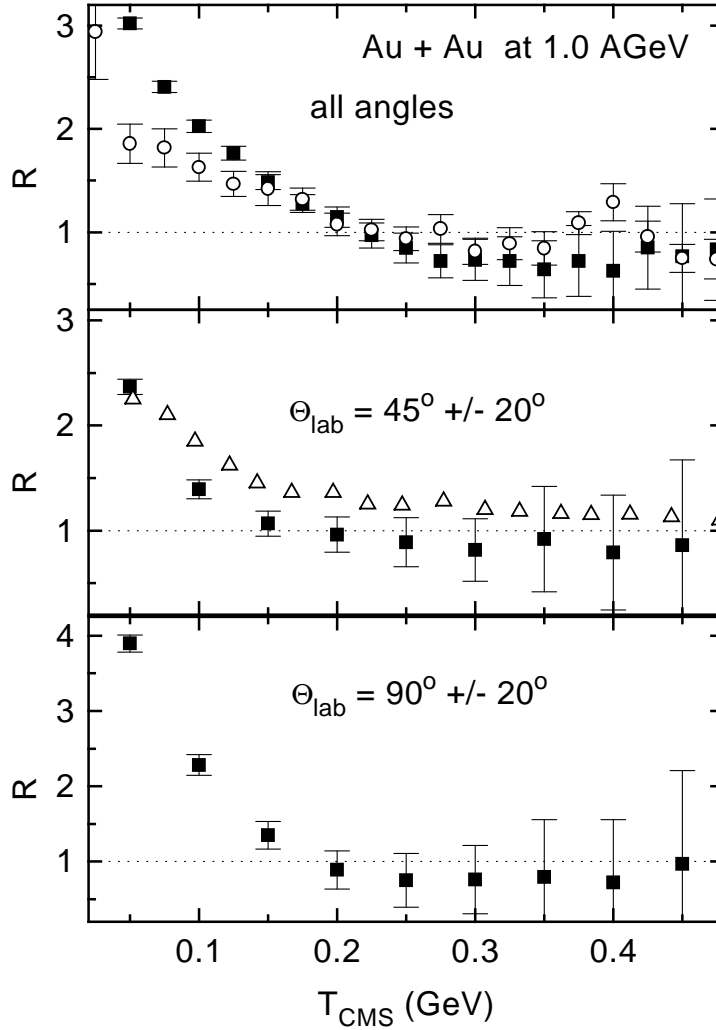


Figure 10: The inclusive  $\pi^-/\pi^+$  ratio  $R$  for Au +Au at 1.0 GeV/A and different angular cuts in the laboratory frame as a function of the pion kinetic energy in the CMS (squares). The errorbars indicate the numerical accuracy within the statistics reached. The open circles represent the experimental data of the FOPI-collaboration [21] and the open triangles indicate the experimental data from the KaoS-collaboration [20] for  $40^\circ \leq \Theta_{lab} \leq 48^\circ$ .

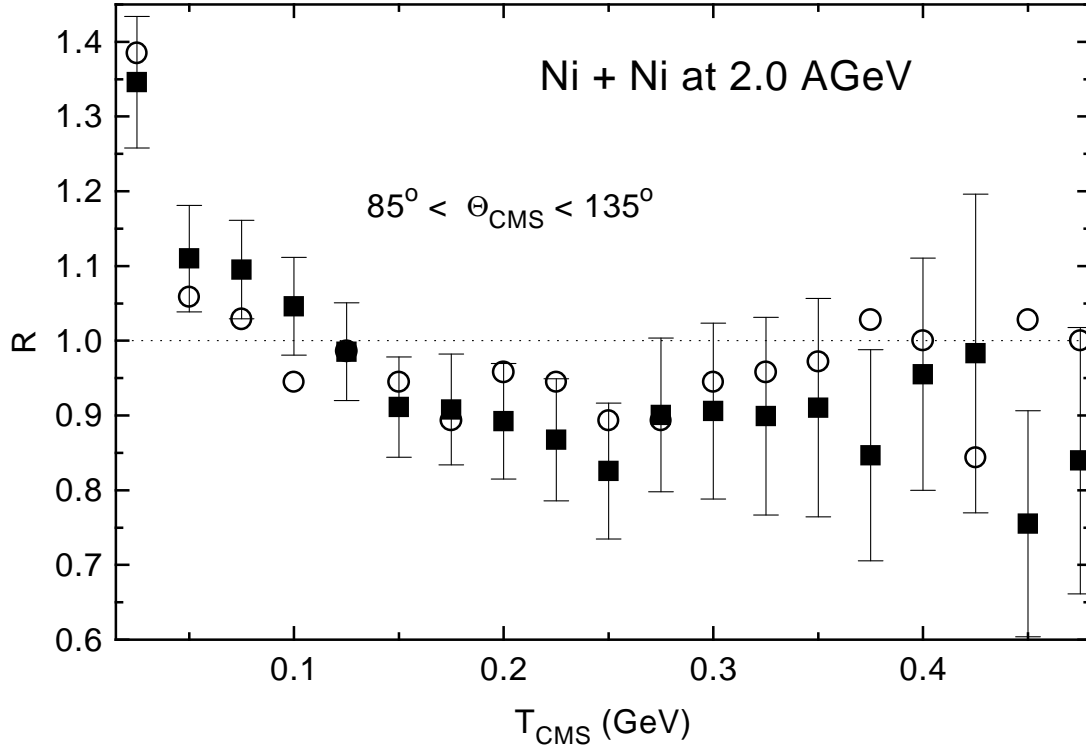


Figure 11: The inclusive  $\pi^-/\pi^+$  ratio  $R$  for Ni + Ni at 2.0 GeV/A as a function of the pion kinetic energy in the CMS for  $85^\circ < \Theta_{CMS} < 135^\circ$ . The solid squares represent the results of the CBUU-calculation; the errorbars indicate the numerical accuracy within the statistics reached. The open circles represent the data obtained by the FOPI-collaboration [22] for a beam energy of 1.93 GeV/A.

- [1] A. Agakichiev et al., Phys. Rev. Lett. **75** (1995) 1272.
- [2] M. A. Mazzoni et al., Nucl. Phys. **A566** (1994) 95c.
- [3] G. Q. Li, C. M. Ko, G. E. Brown, Phys. Rev. Lett. **75** (1995) 4007.
- [4] QUARK MATTER 95, Nucl. Phys. **A590** (1995) .
- [5] W. Cassing, W. Ehehalt and C. M. Ko, Phys. Lett. **B363** (1995) 35.
- [6] Gy. Wolf, W. Cassing, U. Mosel and M. Schäfer, Nucl. Phys. **A517** (1990) 615.
- [7] Gy. Wolf, W. Cassing, and U. Mosel, Nucl. Phys. **A552** (1993) 549.
- [8] Ch. Mntz, PhD Thesis, GSI Report 93-43 (1993).
- [9] St. A. Bass, C. Hartnack, H. Stöcker and W. Greiner, Phys. Rev. **C51** (1995) 3343.
- [10] B. A. Li, Phys. Lett. **B346** (1995) 5.
- [11] S. Teis, W. Cassing, M. Effenberger, A. Hombach, U. Mosel and Gy. Wolf, Z. Phys. **A**, in press; nucl-th/9609009.
- [12] G. F. Bertsch and S. Das Gupta, Phys. Rep. **160** (1988) 189.
- [13] W. Cassing, K. Niita and S.J. Wang, Z. Phys. **A331** (1988) 439.
- [14] W. Cassing, V. Metag, U. Mosel and K. Niita, Phys. Rep **188** (1990) 363.
- [15] R. Stock, Phys. Rep. **135** (1986) 259.
- [16] K. Weber, B. Blättel, W. Cassing, H.-C. Dönges, V. Koch, A. Lang, and U. Mosel, Nucl. Phys. **A539** (1992) 713; K. Weber, B. Blättel, W. Cassing, H.-C. Dönges, A. Lang, T. Maruyama and U. Mosel, Nucl. Phys. **A552** (1993) 571
- [17] R. S. Varga, Matrix iterative analysis, Prentice Hall 1962.
- [18] J. Stoer and R. Burlirsch, Vol. 1, Springer-Verlag, Berlin, (1978).
- [19] C. Mntz et al., Z. Phys. **A352**, (1995), 352.
- [20] C. Mntz et al., Proc. of the international workshop XXIII on gross properties of nuclei and nuclear excitations, Hirschegg, Austria, (1995), p. 345.
- [21] D. Pelte, E. Hfele, D. Best et al., Z. Phys. **A**, in press.
- [22] D. Pelte et al., Z. Phys. **A**, in press.
- [23] W. Ehehalt, W. Cassing, A. Engel, U. Mosel and Gy. Wolf, Phys. Lett. **B298** (1993) 31.